Validation of a structural candidate for γ-N_2 by synchrotron far-infrared spectroscopy

Philip Dalladay-Simpson [1,*] Francesco Capitani [2] and Federico Aiace Gorelli [1,3,4,†]
[1] *Center for High Pressure Science and Technology Advanced Research, 1690 Cailun Road, Shanghai, 201203, China*
[2] *Synchrotron SOLEIL, L'Orme des Merisiers, Départementale 128, 91192 Saint-Aubin, France*
[3] *Instituto Nazionale di Ottica, Consiglio Nazionale delle Ricerche (CNR-INO), 50019 Sesto Fiorentino, Italy*
[4] *Shanghai Advanced Research in Physical Sciences (SHARPS), Shanghai, China*

(Received 10 March 2025; revised 24 April 2025; accepted 2 June 2025; published 8 July 2025)

Nitrogen, known for its rich polymorphism and kinetic barriers, has served as a valuable testbed for evaluating advanced computational methods. In this study, we investigate the infrared absorptions of γ-N_2, a crystalline molecular configuration that is only accessible via a low-temperature compression, employing synchrotron radiation. Our results reveal that γ-N_2 possesses a simple infrared spectrum consisting of only three far-infrared phononic absorptions: a prominent asymmetric peak made up of two unresolved modes, and a weak higher-frequency peak, all of which could be tracked up to 93 GPa. Critically, no absorption associated with an internal vibrational mode of the N_2 molecule was detected up to the highest pressures. Density functional theory (DFT) simulations conducted at 40 GPa demonstrate that these observations align with the $P2_1/c$ structural model, reinforcing its compatibility as a candidate complimenting existing Raman and x-ray diffraction results. Finally, our findings, in conjunction with measurements made over 50 years ago, further support that the formerly assigned "anomalous"/λ N_2-phase is in fact the long-established γ-N_2 phase.

DOI: 10.1103/q4v6-v7y7

I. INTRODUCTION

Simple molecules exhibit rich polymorphism under compression due to the interplay of inter/intramolecular interactions, entropy, and packing efficiencies as they seek configurations that minimize their Gibbs free energy. Nitrogen is an excellent example, showcasing more than 10 distinct molecular configurations, with ι-N_2 demonstrating the extreme complexity possible for such simple diatomic molecular units [1]. However, in contradiction to other elemental diatomic molecular systems, O_2, H_2, and the halogens, N_2 stands alone in the fact that it is found to be susceptible to kinetic barriers [2–5]. This was first evidenced by the existence of an extended polymeric and amorphous structure at high pressures, η-N_2 [2], and secondly pressure-temperature (P-T) path-dependent phase diagram [4–6]. The latter, which also presents as significant metastability—evidenced by multiple phases occupying similar stability fields—makes the nitrogen equilibrium phase diagram difficult to constrain and ultimately elusive to this day.

Recent advancements in single-crystal methodologies through the application of high temperatures have provided unprecedented insight into the molecular configurations of solid nitrogen [1,7,8]. When integrated with state-of-the-art numerical simulations, these advancements can, for the first time, probe nitrogen's equilibrium phase diagram [9]. However, γ-N_2 a molecular configuration formed only through low-temperature compression [6,10–13], does not readily lend itself to single-crystal analysis particularly because of its tendency to form quenchable high-temperature polymorphs [6,13]. As a result, despite being observed over half a century ago [10], its structure to date has only been tentatively assigned via powder x-ray diffraction to a $P2_1/c$ configuration, based on the agreement between diffraction data and low-enthalpy candidate models [6,14,15]. This assignment has recently been further supported by density functional theory (DFT) simulations including many-body interactions and a quasi-harmonic approximation (QHA), which demonstrated reasonable agreement between computed Raman activity and cross sections of this $P2_1/c$ candidate [16] with experimental observations [6]. Nevertheless, fundamental issues with this assignment remain such as the number of Raman-active vibrational modes observed [6,9,17] as well as conflicts with existing structural studies [18]. In addition, the similarity in Raman activity among these candidate structures can also render the assignment ambiguous [8]. Therefore, in the absence of direct techniques to probe the structure, critical additional complimentary spectroscopic information, such as the infrared activity of γ-N_2, is required to provide a more rigorous test of the $P2_1/c$ candidate's validity.

In this study, we investigated the infrared activity of γ-N_2 utilizing synchrotron radiation at pressures approaching 1 Mbar. Our findings reveal a remarkably simple spectrum for γ-N_2, characterized by only three peaks in the far-infrared spectral range, whereas no molecular vibrational absorption is detectable in the mid-infrared range. The observed absorptions include a distinct principal peak with asymmetry—indicative of modes near degeneracy—and a weak higher-frequency feature, all exhibiting pressure-dependent behavior typical of molecular crystals. Our

*Contact author: philip.dalladay-simpson@hpstar.ac.cn
†Contact author: federico.gorelli@hpstar.ac.cn

observations align well with DFT-simulated infrared activity at 40 GPa for the $P2_1/c$ structural model, corroborating existing Raman and x-ray diffraction results [6]. By incorporating measurements from nearly half a century ago [19,20], we provide evidence that the so-called "anomalous"/λ-N_2 [6,12] is indeed γ-N_2 [13], representing a normal (not metastable) dominant phase in nitrogen's phase diagram. The spectroscopic activity observed, combined with numerical computations, provides critical insights for constraining the equilibrium solid molecular phase diagram of nitrogen.

II. EXPERIMENTAL METHODS

Symmetric diamond-anvil cells (DACs) were utilized to generate the high pressures required for this study. Type-IIas diamonds with culets 200 μm in diameter and a Boehler-Almax (BA) design allowing for an optical opening of approximately 70° (4θ). 250-μm-thick Rhenium foils were utilized as gaskets, featuring laser-drilled holes approximately initially 120 μm in diameter and preindented to 30 μm in thickness. High-purity nitrogen (99.99% min.) was gas-loaded into the diamond anvil cell at 1.7 kbar. Upon compression, due to the compressibility and solidification of N_2, the resulting sample chamber measured approximately 100 μm in diameter. Throughout the experiment, the applied load was generated using pressurized helium gas and a metallic-foil membrane.

γ-N_2 was synthesized by compressing the loaded nitrogen gas at low temperatures (67 K) with very low initial pressures (<0.5 GPa) using a custom-built dry cryostat. γ-N2 was formed at 1.1 GPa and compressed up to 30 GPa. This target pressure was selected because γ-N_2 is known to remain stable at room temperature and will not transform into the more entropically favored ϵ-N_2 phase [13]. During the cold compression and subsequent room-temperature compression, pressure was primarily monitored via ruby fluorescence [21] with associated temperature corrections [22] and cross-checked using the Raman-active phonon of the stressed diamond edge [23].

Raman spectroscopy was performed utilizing a custom micro-focused confocal optical system. Raman scattering was excited with a laser wavelength of 532 nm, producing a spot size of approximately 2 μm in diameter using a 0.42 NA objective. To prevent unwanted sample heating during measurements, the incident-laser power was maintained below 5 mW. The backscattered light was collected and filtered through ultra-narrow notch filters before being dispersed by a 320-mm aberration-corrected spectrometer and imaged using a liquid N_2-cooled charge-coupled device (CCD) detector. A 1200 gr/mm grating was employed with CCD exposure times of up to 5 minutes in order to reach a suitable spectral resolution and signal-to-noise ratio. No background subtraction was applied for the data analysis, and the Raman spectra underwent a Bose-Einstein population correction [24] for a temperature of 67 K and are presented in Fig. 1.

Synchrotron infrared measurements were conducted at the SMIS beamline using a homemade horizontal microscope in a transmission configuration and are presented in Fig. 2. Synchrotron infrared radiation was crucial for this study given the higher brightness over conventional IR light sources in the far-infrared range. Long-working-distance custom Schwarzschild

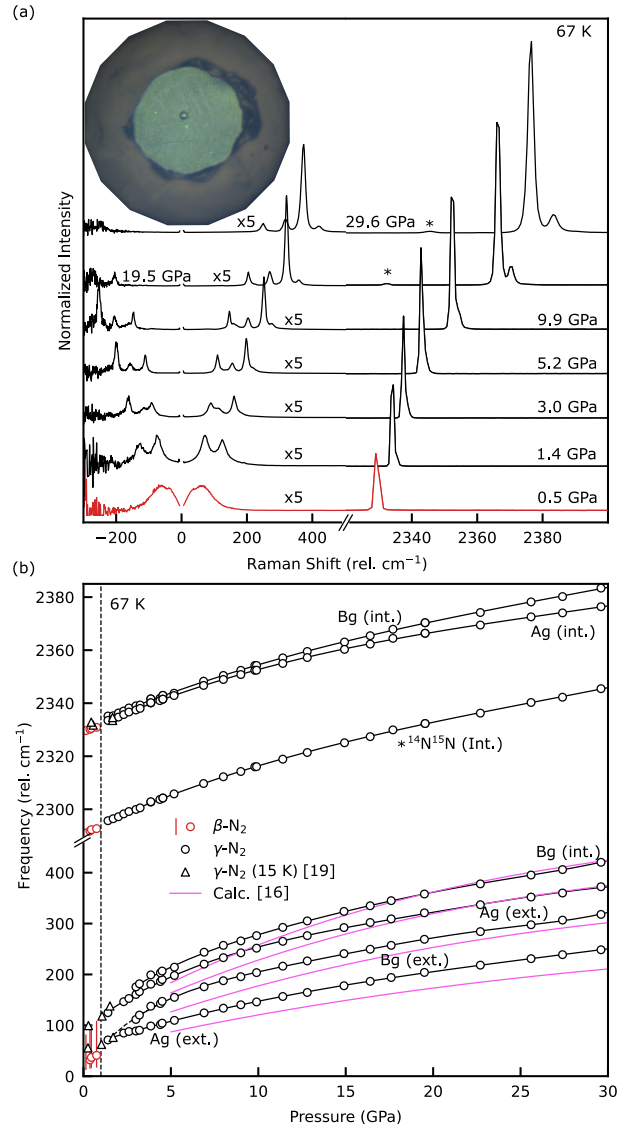

FIG. 1. Raman measurements on γ-N_2 at 67 K up to 30 GPa. (a) Representative Raman spectra, corrected for the Bose-Einstein population factor for a temperature of 67 K [24], resulting in symmetric spectra around the Rayleigh line. The spectra have been cut between–5 cm^{-1} to 5 cm^{-1} as this region is dominated by artifacts arising from the holographic-notch filters. In this panel, red and black traces correspond to β-N_2 and γ-N_2 phases, respectively. The asterisk (*) highlights a weak feature attributed to the isotopic $^{14}N\,^{15}N$ molecular impurity [29,30]. The inset is a micrograph of γ-N_2 at 30 GPa and 67 K, with the sample chamber measuring 100 μm in diameter, approximately half that of the diamond culet. (b) Raman frequencies of nitrogen as a function of pressure during compression at 67 K. Red and black empty circles represent the Raman activity measured in this study of β-N_2 and γ-N_2, respectively. The red bars indicate the full width at half maximum (FWHM) of the broad Raman band, which arises from molecular-orientational disorder of β-N_2. Empty triangles are measurements by Buchsbaum *et al.* on γ-N_2 at 15 K [19]. Magenta traces are from high-level simulation methods of Raman-active modes incorporating many-body interactions with quasi-harmonic approximation density functional theory of the $P2_1/c$ candidate model [16]. The symmetries and nature, whether internal (int.) or external (ext.), of the Raman modes for γ-N2 are assigned according to the proposed $P2_1/c$ model.

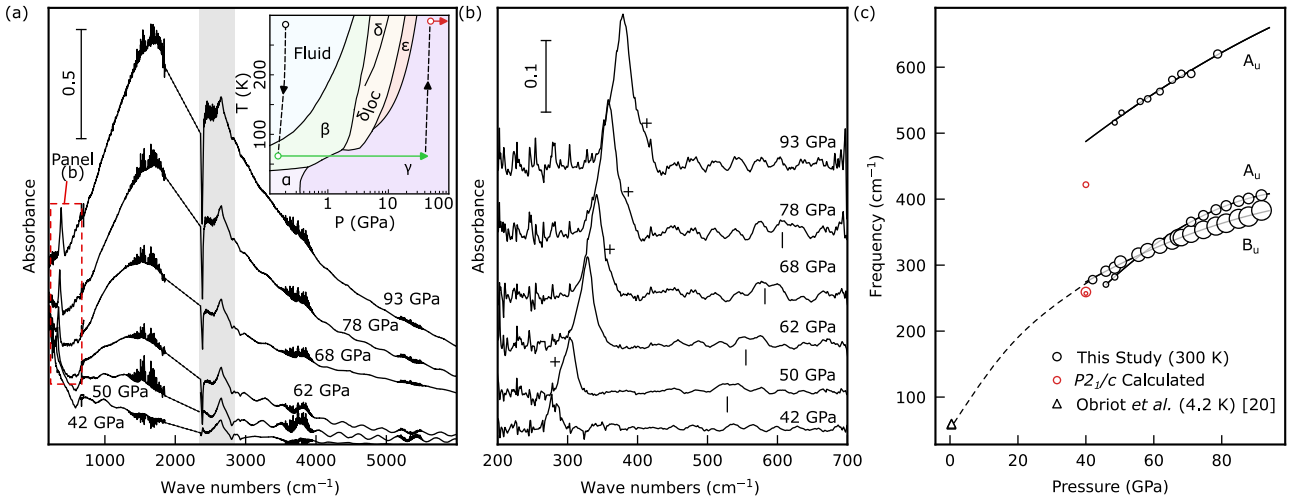

FIG. 2. Synchrotron infrared spectroscopy of γ-N_2 at pressures in the range 42–93 GPa. (a) Selected far- and mid-infrared absorption spectra, with the dashed box indicating the frequency range selected for panel (b). Branches of narrow peaks observed around 1600 cm^{-1} and 3600 cm^{-1} are absorptions from residual water molecules on the purged optical path. Dashed lines are used to substitute spectral regions where the two-phonon diamond absorption approaches saturation and a gray-shaded area marks a regime dominated by artifacts owing to the stressed diamond. (Inset) Phase diagram including the path-dependent triple point (PDTP) [13] with the P-T path taken in this study indicated; green and red arrows denote Raman measurements (Fig. 1) and infrared measurements on compression, respectively. (b) Selected far-infrared absorption spectrum following baseline subtraction, a weak absorption feature at higher frequencies is highlighted by black ticks and an evolving peak asymmetry by an plus symbol (+). Relative optical densities are indicated by the scale bar present in both panels (a) and (b). Narrow peaks below 350 cm^{-1} are absorption from residual water molecules on the purged optical path. (c) Frequencies of infrared absorptions of γ-N_2 as a function of pressure, where empty circles are measurements from this study with the marker size proportional to the absorption intensity. Empty triangles are measurements from Obriot *et al.* at 4.2 K using a large-volume high-pressure optical cell [20]. Red-empty circles represent calculated absorption frequencies for the candidate $P2_1/c$ structure at 40 GPa, as shown in Fig. 3(a). Furthermore, the infrared-active vibrational symmetries, Au and Bu, are assigned to the experimental data based on this model and their evolution is well described by second-order polynomial fits (black traces).

reflective objectives (0.5 NA) were employed for focusing and collecting the infrared light. The collected light was directed onto either a liquid-He cooled silicon bolometer (100-900 cm^{-1}) or a liquid-N_2-cooled mercury cadmium telluride (MCT) detector (650–6000 cm^{-1}) to measure the far- or mid-infrared spectra, respectively. Interferograms were measured by a Fourier-transform Thermo Fisher iS50 spectrometer with a resolution of 2 cm^{-1}. The whole infrared microscope is under a purged environment to minimize atmospheric contributions. Absorption was calculated using an identical cell as a reference, with the two diamond anvils in contact to minimize the interference fringes produced by the Fabry-Perot cavity of an empty gasket hole.

Density functional theory (DFT) phonon calculations for infrared/Raman activity and cross-sections of the γ-N2 low-enthalpy structural candidates [14] were conducted using the Quantum Espresso package [25,26], hosted on the "Materials Square" cloud-based platform with a cumulative cost of $20. The calculations employed the local density approximation (LDA) exchange-correlation functional and utilized norm-conserving Vanderbilt pseudopotentials [27]. Calculations converged satisfactorily using a cutoff energy of 80 Ry and a K-point sampling using a Monkhorst-Pack grid [28] with dimensions of 6×6×6. The emulated spectra are presented in Fig. 3 with assigned widths that reflect experimental observations; further details can be found in the figure caption.

III. RESULTS AND DISCUSSION

The transition to γ-N_2 was observed at 1.1 GPa and 67 K as significant changes in the Raman signature, shown in Fig. 1. This pressure-temperature path, depicted in Fig. 2(a), was chosen to avoid the formation of δ/δ_{loc}-N_2, which results in an entirely different nitrogen phase diagram [13]. At pressures below 1.1 GPa, the system remains within the stability field of β-N_2, and the Raman spectrum is well described by the hexagonal close-packed (hcp) structure, $P6_3/mmc$ [31]. This structure is characterized by a singular optical phonon (E_{2g} mode) and a broad low-frequency band arising from the molecular orientational disorder, as illustrated by the red spectrum in Fig. 1(a). An additional high-frequency vibrational mode at ∼2290 cm^{-1} is observed, which cannot be accounted for by the hcp molecular lattice; this mode, however, can be attributed to the molecular ^{14}N ^{15}N isotopic impurity owing to the coincidence of the reduced frequency of $^{14}N_2$ [30], which is discussed in more detail later. The β-γ transition is characterized by the appearance of two broad, but readily identifiable lattice modes, accompanied by an abrupt narrowing (∼25%) of the linewidth of the N_2 vibrational mode. In addition, the vibrational mode becomes asymmetric on the transition, owing to an additional higher-frequency B_g component, which has been observed in earlier works [19]. It is a point of interest that the pressure-temperature conditions reported here for the transition are remarkably close to those in the pioneering work

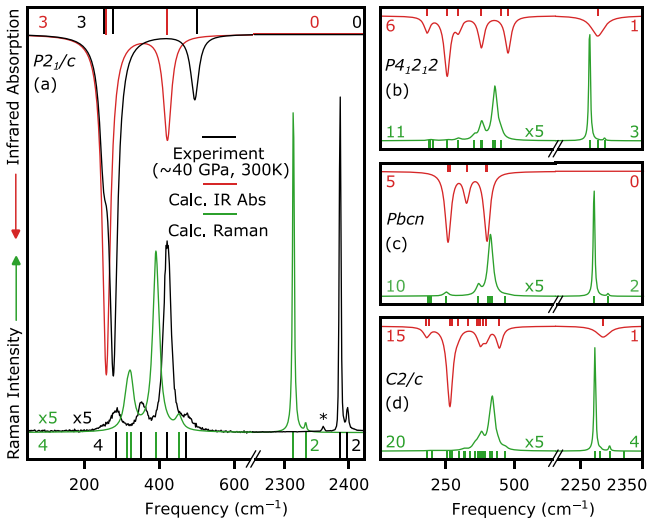

FIG. 3. Density functional theory (DFT) phonon calculations of activity and cross sections of Raman (green trace) and infrared absorption (red trace) of four low-enthalpy candidate structures for γ-N_2 at 40 GPa: (a) $P2_1/c$ (2 molecules/unit cell), (b) $P4_12_12$ structure (4 molecules/unit cell), (c) *Pbcn* structure (4 molecules/unit cell) and (d) $C2/c$ (8 molecules/unit cell). For the simulated spectra, Lorentzian peaks are built upon calculated cross sections and frequencies using widths (FWHM) that reflect experimental observations at 40 GPa: infrared phonons (~25 cm^{-1}), low-frequency Raman excitations (~20 cm^{-1}), and Raman-active vibrational modes (~3 cm^{-1}). Experimental data are included in panel (a) to allow direct comparison with the $P2_1/c$ model. The additional vibrational mode of the isotopic molecular impurity $^{14}N\,^{15}N$ is denoted by an asterisk. The experimental infrared spectrum was reconstructed from extrapolated and observed frequencies, widths and amplitudes for clarity due to the poor signal-to-noise at 40 GPa. Green, red, and black numbers in each panel represent the number of Raman/infrared-active modes for the associated frequency range from simulated Raman, infrared, and experimental observation, respectively

by Stewart, who observed the β-γ transition at 1 GPa and 65 K using direct piston displacement technique [11]. In these early studies, a clear volume discontinuity was observed in the α-γ and β-γ phase transitions identifying them unambiguously to be first order [10,11]. From our vibrational spectroscopy, the mechanism for this transition can be directly attributed to the arresting of molecular rotation, resulting in the orientational ordering of the N_2 molecules in γ-N_2, appearance of lattice modes, from the disordered β-N_2 phase, broad low-frequency band. The β-γ phase transition parallels the well characterised β-α transition at 35 K found at ambient pressure [31]. These are in stark contrast to higher-temperature higher-pressure phase transitions [19,32], where intermediate phases of orientational disorder exist producing "sphere-like" and "disk-like" molecules [33], which in turn plays a critical role in defining the subsequent N_2 phase diagram [13]. In addition, the β-γ transition is found to be remarkably disruptive with the sample becoming heavily textured, as seen in the inset of Fig. 1(a), because of the formation of numerous submicron crystal domains suggesting that single-crystal techniques on bulk samples could be very challenging. Critically, the measurements from this study demonstrate a clear evolution from earlier Raman spectroscopy studies on γ-N_2 up to ~1 GPa and 15 K, shown in Fig. 1(b), a clear indication that we are indeed investigating the same phase of nitrogen, γ-N_2, and previous studies were limited owing to their choice of pressure-temperature pathway [13].

Along the 67 K isotherm, all observed Raman modes exhibit a continuous splitting as a function of pressure, as shown in Fig. 1(b) with no discontinuities indicative of a further phase transition up to 30 GPa. Here, the low-frequency Raman excitations correspond remarkably well with the $P2_1/c$ model, as indicated by the magenta traces, which represent high-level calculations for the $P2_1/c$ model accounting for many-body interactions and a quasi-harmonic approximation [16], supporting the candidacy of this model. Critically, an additional vibrational component is observed both here (highlighted with an asterisk in Figs. 1 and 3) and in previous studies, becoming increasingly prominent at higher pressures [6], which has often led to its dismissal regarding this candidate model [9,17]. Nevertheless, this can be addressed by the inclusion of a naturally abundant molecular isotopic impurity, as mentioned previously for the β-N_2 phase. Two stable isotopes of nitrogen exist: ^{14}N and ^{15}N, with atmospheric abundances of 99.64% and 0.35%, respectively. Therefore, the normal nitrogen utilized in this study consists of three distinct molecular species: $^{14}N\,^{14}N$ ($^{14}N_2$), $^{14}N\,^{15}N$, and $^{15}N\,^{15}N$ ($^{15}N_2$), with relative concentrations of 99.281%, 0.697%, and 0.001%, respectively. Assuming no processes enrich the isotopic fraction of ^{14}N in the process of loading the DAC, we can assume that the relative concentration, and as a consequence the vibrational Raman intensity mirrors that of atmospheric nitrogen gas. Remarkably, although the fraction of $^{14}N\,^{15}N$ molecules is small, <7 ppt, its Raman signature has been observed in previous studies and was rather ingeniously used to probe the intermolecular-coupling constant of solid nitrogen at pressures up to 104 GPa [30]. Interestingly, while the primary focus of this earlier work is on a different phase of nitrogen, namely ϵ-N_2, an "unusual intensity increase" of over 100 times of the impurity $^{14}N\,^{15}N$ vibrational mode relative to the bulk $^{14}N_2$ stretching, with an exponential pressure dependence was noted [30]. This phenomenon parallels the excitation denoted by an asterisk in Fig. 1, where the relative intensities of the assigned $^{14}N\,^{15}N$ and $^{14}N_2$ stretching modes in γ-N_2 no longer reflect their atmospheric abundances. This effect has also been reported in previous studies, but was erroneously assigned as a fundamental vibrational mode of γ-N_2 [6,12,17]. The anomalous intensity enhancement of this isotopic-molecular impurity in γ-N_2 as well as its observation on other N_2 phases [30] is indicative of a more universal behavior. Insight can be gained from the fact that the intensity enhancement appears to depend strongly on the frequency difference between $^{14}N\,^{15}N$ and the $^{14}N(A_g)$ mode, and therefore likely a consequence of an intermolecular-resonance effect between neighboring $^{14}N\,^{15}N$ and $^{14}N_2$ molecules. Similar phenomena have been reported in isotopically mixed solid benzene [34]. The observation of the vibrational mode and its previous erroneous assignment has resulted as a point of dispute with the $P2_1/c$ candidate model [9] or has previously tried to be incorporated as a disorder-activated mode [17].

Synchrotron far-infrared measurements were conducted along a room-temperature isotherm at pressures in the range 40–93 GPa, as shown in the inset of Fig. 2(a). The initial pressure was selected because of the known tendency of γ-N_2 to transform into the entropically favored ϵ-N_2 at pressures below 35 GPa [6]. At 40 GPa, a phononic absorption was observed in γ-N_2 at $\sim$280 cm^{-1}. Although this absorption appears to be relatively weak at this pressure, with an amplitude of $\sim$0.05, the fact that it is observable at all is remarkable. For comparison, previous far-infrared measurements on γ-N_2 at 4.2 K and 0.6 GPa, plotted alongside our measurements in Fig. 2(c), observed a similar absorption for γ-N_2 at 65 cm^{-1}, but for a sample over 750 times thicker (15 mm) [20]. Therefore, there must be an almost three-orders-of-magnitude increase in absorption for γ-N_2 between 0.6 GPa and 40 GPa. On further compression, two additional phononic absorptions were identified both of which are smaller in magnitude. One is found to be near-degenerate, only $\sim$10 cm^{-1} lower in frequency at 46 GPa to the principal absorption in γ-N_2, manifesting as an asymmetric shoulder that evolves into a high-frequency shoulder as pressure increases, as seen in Figs. 2(b) and 2(c). Another absorption becomes identifiable at $\sim$525 cm^{-1} at 50 GPa, with its pressure dependence illustrated in Fig. 2(c). This mode is again smaller in magnitude (0.02) and is comparable to artifact fringes owing to sample thickness making it difficult to identify at all pressure studied.

In the mid-infrared range, no vibrational absorption was detected even up to the highest pressures studied; however, it is important to note that the region characteristic of a N_2 absorption, which is represented by the shaded region in Fig. 2(a), is significantly complicated because of artifacts from stressed diamond, which are not well compensated by the reference taken under no load. On the other hand, clear absorptions have been observed in other nitrogen phases [32] and in our own in-house experiments under similar conditions. Given this, it can be inferred that there is no detectable internal vibrational infrared absorption of N_2 molecules (below an amplitude threshold of 0.05), providing a key constraint for evaluating low-enthalpy candidate structures, as discussed in further detail later. Finally, a strong and broad IR absorption feature was observed, centered around 1600 cm^{-1}, with a remarkable width of 2000 cm^{-1}—exceeding typical vibrational molecular absorptions. Notably, a similar feature has been reported in a higher-pressure nonmolecular nitrogen phase and was attributed to lattice modes [2]. However, given the significant differences in pressure as well as nitrogen phases under investigation between our observations and those of the previous study, it is unlikely that this absorption is an inherent property of nitrogen. Instead, it could be an artifact related to the measurements themselves. Both our study and the previous one are approaching the upper limits of achievable pressures for the diamond-culet geometry, which in turn results in significant elastic deformation of the diamond anvil tip [35]. The stress-strain changes that occur in diamond under these extreme conditions and the associated transmission of light are currently not well understood and could plausibly contribute to this observed artifact.

DFT calculations of Raman and infrared activities and cross sections were performed on low-enthalpy candidate models at 40 GPa, utilizing structural parameters from Ref. [14], which are displayed in Figs. 3(a)–3(d). Focusing solely on Raman activity, the $P2_1/c$ model emerges as the most suitable low-enthalpy candidate, given the presence of low-frequency and stretching modes that match those predicted by the calculations. However, it's important to note that the calculated spectra of all candidate models exhibit qualitative similarities, making the assignment of the $P2_1/c$ model ambiguous and suggesting the need for additional constraints. For instance, although there are significant differences in the number of Raman-active low-frequency modes—20 for $C2/c$ compared to only four for $P2_1/c$—these spectral regions appear almost identical once cross sections are computed and an assigned experimental width shown in Fig. 3. In contrast, far-infrared activity shows significant quantitative differences between the candidate models, presenting an underutilized tool for validating structures through optical spectroscopy. Additionally, compared to the relative Raman cross sections, low-frequency infrared absorptions resulting from lattice and librational motions—key fingerprints for the structure—exhibit significantly stronger amplitudes than their high-frequency counterparts. Given the infrared measurements presented in Fig. 2 and their comparison with simulations in Fig. 3, there is compelling evidence that $P2_1/c$ remains the most suitable candidate for the γ-N_2 phase. Firstly, it is clear the $P4_12_12$ and $C2/c$ candidates can be ruled out as both possess an absorption characteristic of the N_2 stretching (2250–2350 cm^{-1}) that is not observed in our experiments. Meanwhile, although the *Pbcn* structure displays a strong absorption around $\sim$250 cm^{-1}, we would expect another mode of similar amplitude at approximately $\sim$400 cm^{-1}, also ruling out its candidacy. Indeed, a direct comparison with experiments reveals that the calculated infrared spectrum for the $P2_1/c$ model is highly convincing, identifying only three IR-active absorptions with closely matched cross sections, as seen in Fig. 3(a). However, some small discrepancies in frequency and amplitude remain, particularly for the higher-frequency mode ($\sim$15% deviation in frequency), which could likely be addressed by applying a higher level of theory, as was previously in Raman calculations for γ-N_2 [16].

The $P2_1/c$ candidate also exhibits structural characteristics that help to strengthen its candidacy for γ-N_2. Notably, it shares significant parallels with the $P4_12_12$ structure, which has recently been unambiguously assigned to the high-temperature θ-N_2 phase [8]. Both structures consist of layers of canted N_2 molecules arranged in a square 2D lattice, with the molecules aligned perpendicularly to one another between the layers. Consequently, these structures can be classified as polytypes, differing only in the stacking configuration of the layers—AB for $P2_1/c$ and ABCD for $P42_12_12$. As a result, it is not surprising that both phases exhibit remarkably close vibrational properties, as has been discussed in detail by Goncharov *et al.* [8]. However, a conflict remains with early pioneering powder x-ray diffraction measurements suggesting that γ-N_2 corresponds to a $P4_2/mnm$ structure [18]. In their study, the researchers indexed a tetragonal cell using a least-squares method and employed Hartree-Fock estimations to infer structural parameters for the N_2 molecule. While their proposed structure is remarkably similar to the $P2_1/c$ candidate, the key difference lies in the alignment of the

N_2 molecules, which are positioned with their intramolecular axes along the *a*-*b* plane and not canted. However, the authors noted a possibility for the molecules to have a tilt of up to 15° relative to the *a*-*b* plane, making them canted, but opted for the simpler model given qualitative agreement between expected and observed Bragg reflection intensities [18]. Their proposed tilting of the molecules could resolve the conflict with the $P2_1/c$, prompting more direct structural studies at low temperatures. However, it is not unusual for early pioneering powder diffraction works to require revision, particularly as monoclinic distortions can be subtle [36].

IV. CONCLUSIONS

In conclusion, we have investigated the infrared activity of γ-N_2 using synchrotron radiation to pressures approaching 1 Mbar. Our findings reveal a remarkably simple spectrum for γ-N_2, consisting of only three peaks in the far-infrared with no detectable molecular vibrational absorption. Our observations are consistent with DFT-simulated infrared activity at 40 GPa for the $P2_1/c$ structural model, aligning well with existing Raman and x-ray diffraction results [6,15,17]. By incorporating measurements conducted nearly half a century ago [19,20], we provide evidence that the so-called "anomalous"/λ-N_2 [6,12] is indeed γ-N_2 [13], which therefore notably represents a normal (not metastable) dominant phase in nitrogen's phase diagram. The observed spectroscopic activity, coupled with numerical computations, provides crucial insights for constraining the solid molecular phase diagram of nitrogen—elusive since the early 20th century.

ACKNOWLEDGMENTS

The authors acknowledge SOLEIL synchrotron and the SMIS beamline for their support during the experiments conducted under Proposal No. 20240376.

DATA AVAILABILITY

The data that support the findings of this article are not publicly available. The data are available from the authors upon reasonable request.

[1] R. Turnbull, M. Hanfland, J. Binns, M. Martinez-Canales, M. Frost, M. Marqués, R. T. Howie, and E. Gregoryanz, Unusually complex phase of dense nitrogen at extreme conditions, Nat. Commun. **9**, 4717 (2018).

[2] A. F. Goncharov, E. Gregoryanz, H. K. Mao, Z. Liu, and R. J. Hemley, Optical evidence for a nonmolecular phase of nitrogen above 150 GPa, Phys. Rev. Lett. **85**, 1262 (2000).

[3] E. Gregoryanz, A. F. Goncharov, R. J. Hemley, and H.-K. Mao, High-pressure amorphous nitrogen, Phys. Rev. B **64**, 052103 (2001).

[4] E. Gregoryanz, A. F. Goncharov, R. J. Hemley, H.-K. Mao, M. Somayazulu, and G. Shen, Raman, infrared, and x-ray evidence for new phases of nitrogen at high pressures and temperatures, Phys. Rev. B **66**, 224108 (2002).

[5] M. I. Eremets, A. G. Gavriliuk, I. A. Trojan, D. A. Dzivenko, and R. Boehler, Single-bonded cubic form of nitrogen, Nat. Mater. **3**, 558 (2004).

[6] M. Frost, R. T. Howie, P. Dalladay-Simpson, A. F. Goncharov, and E. Gregoryanz, Novel high-pressure nitrogen phase formed by compression at low temperature, Phys. Rev. B **93**, 024113 (2016).

[7] D. Laniel, F. Trybel, A. Aslandukov, J. Spender, U. Ranieri, T. Fedotenko, K. Glazyrin, E. L. Bright, S. Chariton, V. B. Prakapenka *et al.*, Structure determination of ζ-N_2 from single-crystal x-ray diffraction and theoretical suggestion for the formation of amorphous nitrogen, Nat. Commun. **14**, 6207 (2023).

[8] A. F. Goncharov, I. G. Batyrev, E. Bykova, L. Brüning, H. Chen, M. F. Mahmood, A. Steele, N. Giordano, T. Fedotenko, and M. Bykov, Structural diversity of molecular nitrogen on approach to polymeric states, Phys. Rev. B **109**, 064109 (2024).

[9] M. Kirsz, C. G. Pruteanu, P. I. C. Cooke, and G. J. Ackland, Understanding solid nitrogen through molecular dynamics simulations with a machine-learning potential, Phys. Rev. B **110**, 184107 (2024).

[10] C. A. Swenson, New modification of solid nitrogen, J. Chem. Phys. **23**, 1963 (1955).

[11] J. W. Stewart, Compression of solidified gases to 20,000 kg/cm2 at low temperature, J. Phys. Chem. Solids **1**, 146 (1956).

[12] H. E. Lorenzana, M. J. Lipp, and W. J. Evans, Anomalous molecular phase of nitrogen: Implications to the phase diagram, High Press. Res. **22**, 5 (2002).

[13] J. Yan, P. Dalladay-Simpson, L. J. Conway, F. Gorelli, C. Pickard, X.-D. Liu, and E. Gregoryanz, Remarkable stability of γ-N_2 and its prevalence in the nitrogen phase diagram, Sci. Rep. **14**, 16394 (2024).

[14] C. J. Pickard and R. J. Needs, High-pressure phases of nitrogen, Phys. Rev. Lett. **102**, 125702 (2009).

[15] C. Fan, S. Liu, J. Liu, B. Wu, Q. Tang, Y. Tao, M. Pu, F. Zhang, J. Li, X. Wang *et al.*, Evidence for a high-pressure isostructural transition in nitrogen, Chin. Phys. Lett. **39**, 026401 (2022).

[16] W. Sontising and G. J. O. Beran, Theoretical assessment of the structure and stability of the λ phase of nitrogen, Phys. Rev. Mater. **3**, 095002 (2019).

[17] S. Liu, M. Pu, Q. Tang, F. Zhang, B. Wu, and L. Lei, Raman spectroscopy and phase stability of λ-N_2, Solid State Commun. **310**, 113843 (2020).

[18] R. L. Mills and A. F. Schuch, Crystal structure of gamma nitrogen, Phys. Rev. Lett. **23**, 1154 (1969).

[19] S. Buchsbaum, R. L. Mills, and D. Schiferl, Phase diagram of N_2 determined by Raman spectroscopy from 15 to 300 K at pressures to 52 GPa, J. Phys. Chem. **88**, 2522 (1984).

[20] J. Obriot, F. Fondere, and P. Marteau, An apparatus for far-infrared absorption of molecular solids at liquid Helium temperature and high pressure, Infrared Phys. **18**, 607 (1978).

[21] G. Shen, Y. Wang, A. Dewaele, C. Wu, D. E. Fratanduono, J. Eggert, S. Klotz, K. F. Dziubek, P. Loubeyre, O. V. Fat'yanov *et al.*, Toward an international practical pressure scale: A proposal for an IPPS Ruby gauge (IPPS-Ruby2020), High Press. Res. **40** 299 (2020).

[22] F. Datchi, A. Dewaele, P. Loubeyre, R. Letoullec, Y. Le Godec, and B. Canny, Optical pressure sensors for high-pressure-high-temperature studies in a diamond anvil cell, High Press. Res. **27**, 447 (2007).

[23] Y. Akahama and H. Kawamura, Pressure calibration of diamond anvil Raman gauge to 310 GPa, J. Appl. Phys. **100**, 043516 (2006).

[24] T. H. Kauffmann, N. Kokanyan, and M. D. Fontana, Use of Stokes and anti-Stokes Raman scattering for new applications, J. Raman Spectrosc. **50**, 418 (2019).

[25] P. Giannozzi, S. Baroni, N. Bonini, M. Calandra, R. Car, C. Cavazzoni, D. Ceresoli, G. L. Chiarotti, M. Cococcioni, I. Dabo *et al.*, Quantum Espresso: A modular and open-source software project for quantum simulations of materials, J. Phys.: Condens. Matter **21**, 395502 (2009).

[26] P. Giannozzi, O. Andreussi, T. Brumme, O. Bunau, M. B. Nardelli, M. Calandra, R. Car, C. Cavazzoni, D. Ceresoli, M. Cococcioni *et al.*, Advanced capabilities for materials modelling with Quantum Espresso, J. Phys.: Condens. Matter **29**, 465901 (2017).

[27] D. R. Hamann, Optimized norm-conserving Vanderbilt pseudopotentials, Phys. Rev. B **88**, 085117 (2013).

[28] H. J. Monkhorst and J. D. Pack, Special points for Brillouin-zone integrations, Phys. Rev. B **13**, 5188 (1976).

[29] J. Yamamoto and Y. Hagiwara, Precision evaluation of nitrogen isotope ratios by Raman spectrometry, Anal. Sci. Adv. **3**, 269 (2022).

[30] H. Olijnyk and A. P. Jephcoat, Vibrational dynamics of isotopically dilute nitrogen to 104 GPa, Phys. Rev. Lett. **83**, 332 (1999).

[31] T. H. Jordan, H. Warren Smith, W. E. Streib, and W. N. Lipscomb, Single-crystal x-ray diffraction studies of α-N_2 and β-N_2, J. Chem. Phys. **41**, 756 (1964).

[32] R. Bini, L. Ulivi, J. Kreutz, and H. J. Jodl, High-pressure phases of solid nitrogen by Raman and infrared spectroscopy, J. Chem. Phys. **112**, 8522 (2000).

[33] G. W. Stinton, I. Loa, L. F. Lundegaard, and M. I. McMahon, The crystal structures of δ and δ* nitrogen, J. Chem. Phys. **131**, 104511 (2009).

[34] E. R. Bernstein, Site effects in isotopic mixed crystals-site shift, site splitting, orientational effect, and intermolecular Fermi resonance in the vibrational spectrum of benzene, J. Chem. Phys. **50**, 4842 (1969).

[35] B. Li, C. Ji, W. Yang, J. Wang, K. Yang, R. Xu, W. Liu, Z. Cai, J. Chen, and H.-K. Mao, Diamond anvil cell behavior up to 4 Mbar, Proc. Natl. Acad. Sci. USA **115**, 1713 (2018).

[36] K. Takemura, H. Fujihisa, Y. Nakamoto, S. Nakano, and Y. Ohishi, Crystal structure of the high-pressure γ phase of mercury: A novel monoclinic distortion of the close-packed structure, J. Phys. Soc. Jpn. **76**, 023601 (2007).